Heliyon 5 (2019) e02193

Contents lists available at ScienceDirect

Heliyon

journal homepage: www.heliyon.com

Simulation-based protein engineering of *R. erythropolis* FMN oxidoreductase (DszD)

Ramin Fallahzadeh [a], Bijan Bambai [b,*], Kasra Esfahani [b], Abbas Akhavan Sepahi [a]

[a] *Microbiology and Biotechnology Research Group, Tehran North Branch of Islamic Azad University, Tehran, Iran*
[b] *National Institute for Genetic Engineering and Biotechnology (NIGEB), Tehran, Iran*

ARTICLE INFO

Keywords:
Bioinformatics
Biocomputational Method
Biotechnology
Microbial Biotechnology
Molecular Biology
Specific activity
Rhodococcus erythropolis IGTS8
molecular dynamics simulations
DszD enzyme
MM-PBSA method

ABSTRACT

The sulfur contents of fossil fuels have negative impacts on the environment and human health. The bio-catalytic desulfurization strategies and the biological refinement of fossil fuels are a cost-effective process compared to classical chemistry desulfurization. *Rhodococcus erythropolis* IGTS8 is able to metabolize the organic sulfur compound by the unique genes cluster (i.e. DszA, B, C and D genes) in the 4S metabolic pathway. The *dszD* gene codes a key enzyme for sulfur reduction in the gene cluster. In this study, the structure of the DszD enzyme was predicted and then the key residues toward FMN binding were identified which were Thr62, Ser63, Asn77, and Ala79. To investigate the effect of manipulation in key residues on the enzymatic activity of the DszD, different mutations were performed on key residues. The molecular docking simulation showed that A79I and A79N mutants have the lowest binding free energies compared to the wild-type enzyme in binding with FMN substrate. A 50 ns molecular dynamics (MD) simulation performed using GROMACS software. The RMSD and RMSF analysis showed that two mutants are more stable than the wild-type enzyme during MD simulation. The binding free energies between FMN substrate and complexes were calculated and analyzed by the Molecular Mechanics/Poisson-Boltzmann Surface Area (MM-PBSA) method. The experimental results showed that the enzyme activity for the oxidoreductase process toward biodesulfurization increased 1.9 and 2.3 fold for A79I and A79N mutants, respectively.

1. Introduction

Combustion of the fossil fuels releases toxic sulfur dioxide into the environment which causes several problems including acid rain, air pollution and subsequent many health problems to human (Kilbane, 2006; Etemadi et al., 2018). Crude oil contains a large number of molecules having sulfur. However, alkylated dibenzothiophenes (DBT) is the largest portion of sulfur-containing compounds in petroleum derivatives (Nuhu, 2013; Chen et al., 2018). To decrease the level of sulfur dioxide released to the atmosphere, it is necessary to decrease the sulfur in the fossil fuels (Morrison et al., 2013; Etemadi et al., 2018). There are different methods to remove the polycyclic sulfur from fossil fuels. Among them, hydrodesulfurization (HDS) is the most commonly used method (Gupta et al., 2005; Akhtar et al., 2016; Etemadi et al., 2018). Hydrodesulfurization process can easily omit the inorganic sulfur, but because of their remarkable conflicts with hydrodesulfurization, this process is not sufficient for eliminating the polycyclic sulfur derivatives (Davoodi-Dehaghani et al., 2010). Moreover, besides the harsh operational conditions including high temperatures and pressure, it needs high cost and also this process generates the hazardous H_2S gas (Martínez et al., 2017; Nazari et al., 2017).

Because of the above-mentioned shortages, during the last decades, several attempts have been made in developing alternatives to hydrodesulfurization including oxidative desulfurization (Zhang et al., 2013), adsorptive desulfurization (Xiao et al., 2013) and biodesulfurization (Borzenkova et al., 2013). Among these methods, biodesulfurization (BDS) is one of the main methods which eliminate the polycyclic sulfur from oil fractions via microorganisms without breaking down the carbon skeleton of the polycyclic sulfur derivatives or reduction of the energetic value of fuel (Sucharitakul et al., 2014; Etemadi et al., 2018).

The discovery of anaerobic sulfur-specific pathway, 4S pathway, in the Gram-positive *Rhodococcus erythropolis* IGTS8 strain (ATCC 53968) is known as a turning point on biodesulfurization, because it is a non-destructive pathway which retains the full combustion capacity of fossil fuel (Karimi et al., 2018). According to this pathway, sulfur is removed selectively, whereas the carbon skeleton and the caloric value of the

* Corresponding author.
E-mail address: bambai@nigeb.ac.ir (B. Bambai).

https://doi.org/10.1016/j.heliyon.2019.e02193
Received 16 February 2019; Received in revised form 28 June 2019; Accepted 29 July 2019
2405-8440/© 2019 Published by Elsevier Ltd. This is an open access article under the CC BY-NC-ND license (http://creativecommons.org/licenses/by-nc-nd/4.0/).

resulting S-free 2-hydroxybiphenyl (2HBP) end product remain intact (Chen et al., 2018). The 4S pathway transforms DBT into 2HBP and sulfite by four subsequent reactions catalyzed by DszC (DBT monooxygenase), DszA (DBT-sulfone monooxygenase) and DszB (2-hydroxybiphenyl-2-sulfinate (HBPS) desulfinase) enzymes. These enzymes are codified by the *dszC, dszA* and *dszB* genes, respectively, which are part of the *dszABC* operon located in a 120 kb plasmid in strain IGTS8 (Nielsen et al., 2010; Khosravinia et al., 2018). An NADH dependent FMN oxidoreductase, DszD enzyme, encoded by the chromosomally-located *dszD* gene, provides $FMNH_2$ required for the activities of DszC and DszA enzymes. The DszD enzyme with 192 residues and a molecular weight of ~22 kD is a key enzyme which is proposed to be responsible for the rate-limiting step of the 4S pathway (Sousa et al., 2016).

A drawback to large-scale application of biodesulfurization in biorefineries is its low process rate. To enhance the yield and rate of bacterial desulfurization, one of the key factors is to manipulate the genes involved in the biodesulfurization pathway. We were interested to investigate the effect of manipulation in key residues on the enzymatic activity of the DszD enzyme. So, in the present study, first, we determined the 3D structure and also the key residues for the specific binding site of FMN substrate on DszD enzyme through homology modeling. Then the point mutagenesis in the key residues was performed and the best mutants were selected by docking and molecular dynamic simulation. Finally, the cloning, expression and activity assay were performed on the selected mutants to evaluate the enzyme activity.

2. Material & methods

2.1. Structural prediction of DszD enzyme

Due to the unavailable crystallographic structure of DszD enzyme, the CPH-models server (Nielsen et al., 2010), was used for structural modeling. The amino acids sequence of DszD was obtained from the NCBI protein sequence database (GenBank: AAC38226.1). In this study, homology modeling was applied for structural prediction and recognition of FMN binding sites in the enzyme. In homologues identification procedure, the sequences with highest identities were selected as templates in the protein data bank (PDB) for recognition of critical amino acids in binding with the FMN substrate. The Chimera software version 1.10.1 was employed for visualizing the templates and the predicted model (DszD enzyme). Furthermore, the 4XJ2 protein showed the most superimposable active site among all templates. The sequence identity and sequence similarity between 4XJ2 and DszD enzyme is 38% and 67%, respectively. The Swiss PDB Viewer software (Kaplan and Littlejohn, 2001) was used to generate mutant structures from the predicted structure at key residues (i.e. at Thr62, Ser63, Asn77, and Ala79). Further, these structures were used to perform molecular docking and MD simulation.

2.2. Molecular docking studies

Molecular docking studies were performed using AutoDock 4.2 program (Morris et al., 2009). The Kollman charges were added to the complexes by AutoDock Tools (ADT) before performing docking calculations. The FMN binding site was centered in the box and a grid box was created with 60 × 50 × 40 points and a grid spacing of 0.375 Å in which almost covered the entire enzyme were involved. Docking simulations were performed using the classical Lamarckian genetic algorithm (LGA). The 20 LGA runs with a maximum of 2500000 energy evaluations performed. In addition, the other parameters were set to default. The pose with lowest binding energy or binding affinity used as starting complex for MD simulation.

2.3. Molecular dynamics simulation of enzyme-substrate complex

After molecular docking, all selected enzyme–substrates complexes (i.e. Enzyme–FMN) were prepared to be studied through the MD simulations. Simulations were carried out using the GROMACS 5.1.2 package (Abraham et al., 2015) and gromos 53a6 force field (Oostenbrink et al., 2004). The Automated Topology Builder (ATB) server (Koziara et al., 2014) also provided gromos 53a6 force field parameters for FMN substrate. All the systems were first solvated in SPC/E water model (Mark and Nilsson, 2001) and neutralized with counter ions in cubic boxes with a length of 7.7 nm. The Periodic Boundary Conditions (PBC) were applied to all axes, short-range electrostatic and van der Waals cut-off was set to 1.2 nm in energy minimization of all the systems using the steepest descent algorithm, LINCS algorithm (Hess, 2008) also used for holonomic constraints of all bonds in NVT and NPT equilibration of the systems.

The particle mesh Ewald (PME) method (Darden et al., 1993) applied in treating long-range electrostatic interactions. The Berendsen thermostat (Berendsen et al., 1984) also applied for temperature coupling at 310K and Parrinello-Rahman algorithm (Parrinello and Rahman, 1981) for pressure coupling at 1 bar in the uniform scaling of box vectors (isotropic). Three independent simulations were performed for 50 ns for each complex. Similar to energy minimization, the short-range electrostatic and van der Waals cut-off was set to 1.2 nm for the 50 ns simulation. All analysis was performed using Gromacs gmx-toolbox. The evolution of the secondary structure of DszD was analyzed using DSSP program (Frishman and Argos, 1995; Kumari et al., 2014).

2.4. Calculation of the binding free energy

The MM-PBSA method with g_mmpbsa script was used to calculate the binding free energy of the wild-type DszD enzyme and its mutant's (E) interaction with the FMN substrate (L) ($\Delta G_{bind} = G_{LE} - G_E - G_L$). The binding free energy (ΔG_{bind}) is obtained by following equation:

$$\Delta G_{bind} = \Delta E_{MM} + \Delta G_{Pol} + \Delta G_{npol} - T\Delta S$$

Where ΔE_{MM} is the molecular mechanical energy consisting of electrostatic (ΔE_{ele}) and van der Waals (ΔE_{vdw}) contributions. ΔG_{Pol} and ΔG_{npol} denote polar and nonpolar solvation energies, respectively. The entropic term ($T\Delta S$) is expected to be similar for DszD structures, and can be neglected (Ferreira et al., 2017). The calculation of energies was performed for the last 30 ns of all MD simulations. The length of the simulation steps was set to 0.2 ns, i.e. 150 snapshots were used totally in the energy calculations and then further averaged over the two replicate simulations (Kumari et al., 2014; Genheden and Ryde, 2015).

2.5. Experimental procedures

2.5.1. Chemicals, bacterial strains, plasmids, and primers

Genomic DNA was obtained from *Rhodococcus erythropolis* IGTS8. The cloning vector and host were pBluescript II KS (+) vector (Fermentas) and *E. coli* DH5a cells (Novagen). Furthermore, the expression of wild-type and mutant enzymes was done by using the pET-23a (+) (Novagen) and *E. coli* BL21 (DE3) (Promega). DNA polymerase, *Bam* HI and *Eco* RI, T4 Ligase, Ampicillin from Roche Diagnostic (Germany); and DNA ladders, protein markers, T4 DNA ligase and anti-T7 tag antibody were purchased from Abcam Company. NADH and FMN sodium salts, and the IPTG- X-Gal were purchased from Sigma Company. The DNA extraction kit and high pure plasmid purification kit were obtained from Qiagen Company. The agarose gel extraction kit and the PCR product purification kit were obtained from the Roche company. The LB medium containing 100 μg/ml ampicillin was used in the benchtop operations at 37 °C.

2.5.2. Construction of expression plasmids

The *dszD* gene amplicon (599 bp) was cloned using *Bam* HI and *Eco* RI sites of the pET-23a (+) expression vector, named pET-dszD plasmid. Then, the *E. coli* BL21 (DE3) cells were transformed with pET-dszD. The

dszD mutants were created using the SOEing-PCR method (Young et al., 2017). The mutagenic primers and the pET-dszD plasmid were applied as a template in the SOEing-PCR method. All molecular biology methods were according to the standard protocol (Sambrook et al., 1989).

2.5.3. Expression of recombinant genes and analysis

The expression vector was pET-23a that was under the control of the T7 promoter. Furthermore, the expression was done in *E. coli* BL21 (DE3) cells. The original start codon of *dszD* (TTG) was replaced by ATG of *E. coli* at the beginning of the forward primer in all genes. The single colonies were selected from wild-type and mutant plates to examine their expression by induction 1 mM IPTG in LB broth medium for 3 h at 37 °C (OD600 of 0.6–0.7). The cells harvested by centrifugation and disrupted by ultra-sonication following suspension in Tris-HCl buffer. The lysates centrifuged at 9000 rpm for 3 min to remove cell debris and supernatants were used for further analysis. Then, the discontinuous SDS-PAGE was performed under reducing conditions with a 12.5% polyacrylamide gel (Schägger, 2006).

2.5.4. Enzyme assay

The assay based on the oxidation of NADH can determine the activity of NADH dependent FMN oxidoreductase (Kamali et al., 2010). The enzyme activities were determined at 25 °C by quantifying the decrease in absorbance at 340 nm. The oxidation of NADH to NAD decreased optical density. The solution of 50 mM Tris/HCl (pH 7.5), 140 μM NADH, 20 μM FMN and varying amounts of cell extract in 1 ml were used an assay mixture. A unit activity is the required amount of flavin reductase to oxidize 1 μM NADH per min ($\varepsilon_{340} = 6.22 \times 10^3\ M^{-1}\ cm^{-1}$). The equal concentration of total proteins was used for the determination of enzyme activity. The protein concentration was determined by the Bradford method (Kruger, 2002) with bovine serum albumin as standard.

3. Results & discussion

3.1. Structural prediction

The amino acid sequence of DszD enzyme (GenBank: AAC38226.1) was retrieved from the NCBI database and its modeling was obtained by the CPHmodels server (Fig. 1). Amino acids sequence of the DszD enzyme was aligned in the Protein Data Bank for finding the most homologous structures. By searching in the protein data bank, 22 homologous proteins were found and after downloading their PDB information, the multiple alignments of these 22 PDB files was done with the DszD.pdb (Fig. 2).

Among all aligned sequences, the homologous sequence containing FMN substrate revealed the key residues at the FMN binding sites in DszD enzyme which were Thr62, Ser63, Asn77, Ala79 residues. Eighteen candidate mutants were created in these key residues (i.e. at the Thr62, Ser63, Asn77, and Ala79 residues).

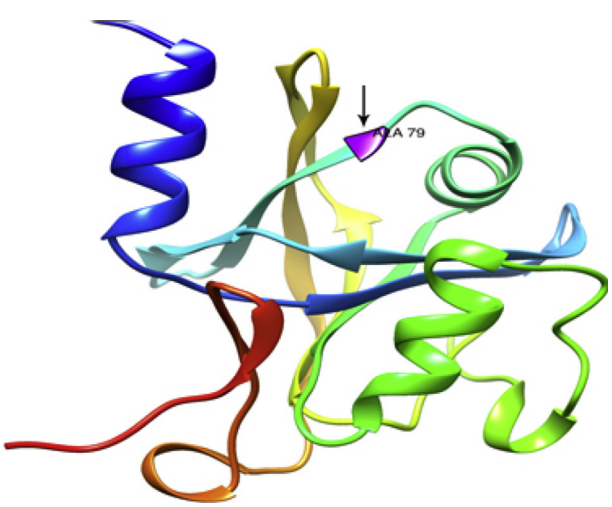

Fig. 1. Predicted three dimensional structure for wild-type DszD enzyme.

3.2. Molecular docking

The FMN substrate was docked to wild-type enzyme and these created mutants in the AutoDock software. As a result, an estimation of the FMN binding free energy (ΔG_{bind}) was obtained (Table 1).

Regarding docking scores, two conformations of mutant enzymes presented the lowest binding energies compared to the free energy of wild-type enzyme in binding with the FMN substrate. These two mutants include of substitution of alanine 79 by isoleucine (A79I mutant) and asparagine (A79N mutant). Interestingly, it was viewed that correspond residues (Asn or Ile residue instead of Ala79) were presented on the 3K88 and 4L82 homologous proteins, respectively (Fig. 2).

3.3. Molecular dynamics simulation of enzyme-substrate complex

To study the influence of mutations on DszD-FMN interaction, we performed All-Atom molecular dynamics (MD) simulation. In this study, 50 ns of MD simulation performed on each wild-type and mutant DszD enzymes in complex with FMN substrate.

3.3.1. Studying the stability of DszD enzyme and mutants

According to Fig. 3, the root-mean-square deviations (RMSD) of Cα atoms of the wild-type DszD enzyme and mutants structures reach a plateau in 25 ns of simulation time and exhibit less conformational changes in the last 15 ns. The calculated average RMSD for A79I and A79N mutants are 0.48 ± 0.05 nm and 0.41 ± 0.03 nm, respectively, which both are smaller than the average RMSD for wild-type (0.49 ± 0.08 nm).

Furthermore, the fluctuation of residues in the FMN-enzyme complex was studied by calculating the root-mean-square fluctuation (RMSF) of the backbone atoms (Fig. 4(A)). The mutated enzymes (A79I and A79N) demonstrate lower values of RMSF compared to wild-type enzyme indicating that asparagine and isolucine are fluctuating in a more limited range than wild-type enzyme (Fig. 4(B)). This observation could be attributed to the chemical structure of the substituted residues. Comparing the chemical structures reveals that an amide group in asparagine is substituted instead of a hydrogen atom in alanine which enables asparagine for stronger interamolecular interactions including hydrogen bonds and hence cause to lower fluctuation. While, comparing the chemical structure of alanine and isoleucine reveals that the methyl group in alanine is substituted by *Sec*-butyl group in isoleucine. Regarding that the of alkyl groups have approximately the same polarity, hence the fluctuation difference between A79I and wild-type is not evident as A79N. Since the overall fluctuation of enzyme is a function of fluctuation of individual residues, it is evident that decreasing the fluctuation in one position will affect the total fluctuation on the enzyme.

The dictionary of the secondary structure of protein (DSSP) analysis is performed to assess the impact of mutations on the secondary structure of the DszD (Fig. 5). DSSP revealed the contribution of each amino acid in the formation of the local secondary structure of protein like (alpha helix, Sheet, Turns, etc) (Kabsch and Sander, 1983; Tripathi et al., 2016). DSSP analysis shows the location of residue 79 in the α-Helix region with any change in the predicted secondary structure of these mutants. It means that residue 79 was located in the α-Helix region in the wild-type enzyme, A79I mutant, and A79N mutant.

Fig. 6 shows the hydrogen bond analysis in FMN and different enzymes complexes at the end of simulation. The number of hydrogen bonds and also their position between FMN and enzymes are shown in this figure. For more clarity, the details of the hydrogen bonds (length and position) are summarized in Table 2.

According to Fig. 6, the mutant enzyme complexes with FMN shows

Fig. 2. The alignment of wild-type DszD enzyme with homologues proteins. The FMN substrate bonds to the key residues (Thr62, Ser63, Asn77 and Ala79) of the wild-type DszD enzyme.

Table 1
Molecular Docking results of the FMN substrate to the wild-type DszD enzyme and mutants.

Enzyme	Binding free energy (kcal/mol)
wild-type DszD	-8.25
T62A	-8.58
T62N	-8.87
T62S	-8.62
T62Q	-8.48
S63A	-8.27
S63T	-8.48
N77A	-8.33
N77C	-8.26
N77F	-8.33
N77G	-8.21
N77S	-8.36
N77V	-8.39
A79Q	-8.82
A79S	-8.37
A79V	-8.66
A79T	-8.76
A79I	-8.99
A79N	-9.77

restricted deviation which proves the stability and this result is in accordance with RMSF results. The helical structure of 62–67 residues turned to coils after ~20 ns of simulation in the wild-type enzyme. However, the helical structure of this region is conserved in two mutations until the end of the simulation which could result in a change in the number of hydrogen bond interactions between its key residues and FMN substrate. To investigate the stability of enzyme-substrate complexes, the total numbers of hydrogen bonds were calculated for three complexes during the 50 ns of simulation (Fig. 7). The H-bond analysis showed that FMN substrate binds more appropriately with A79N mutant through hydrogen bonds which comprise an average of 5.32 H-bond throughout the simulation. Also, the average number of H-bond for A79I mutant is 5.19 throughout the simulation. Since the number of H-bonds for both mutants are greater than wild-type (4.85), so it causes to more stability in FMN-enzyme complex.

3.4. The binding free energy

The binding energies of the three complexes were analyzed by g_mmpbsa script. Regarding the average calculated binding free energy (Table 3), A79N mutant show lower energy in the enzyme-substrate complex, while there is low difference for A79I in that complex. According to the analyzed different types of intermolecular interactions (Table 3), the main difference in the interactions of A79N mutant with FMN substrate is related to the van der Waal energy. The van der Waals energy of A79N mutant is lower than wild-type DszD which means that the substitution of asparagine in Ala79 positions is a favorable mutation. These lowering in van der Waals energy can be attributed to the chemical structures of corresponding residue. Since the van der Waals interactions depend on the momentary dipole-dipole interactions and hence to the molecules size, so by increasing the size of residue (asparagine compared to alanine) the van der Waals interactions are increased for mutant.

The contribution of the mutation at 79 position in total binding free energy is calculated in comparison with wild-type enzyme and demonstrated in Table 4. Regarding the decreased amounts of binding free energy (or stronger interaction between mutant and FMN), it can be concluded that substitution at position 79 by asparagine, favored the binding of A79N mutant enzyme to the FMN substrate.

3.5. Experimental procedures

The wild-type *dszD* gene was amplified using the specific primers DszD-F and DszD-R by PCR procedure. The *dszD* mutant genes were obtained using the SOEing-PCR by mutagenic primers (Table 5). The amplicon fragments from the first and second PCRs were purified and used as templates for the third PCR. The full-length amplicon achieved from the third PCR that was cloned into pET-23a (+) to create recombinant plasmids pET-A79N and pET-A79I. These plasmids carried the DszD mutants A79N and A79I, respectively. These plasmids were

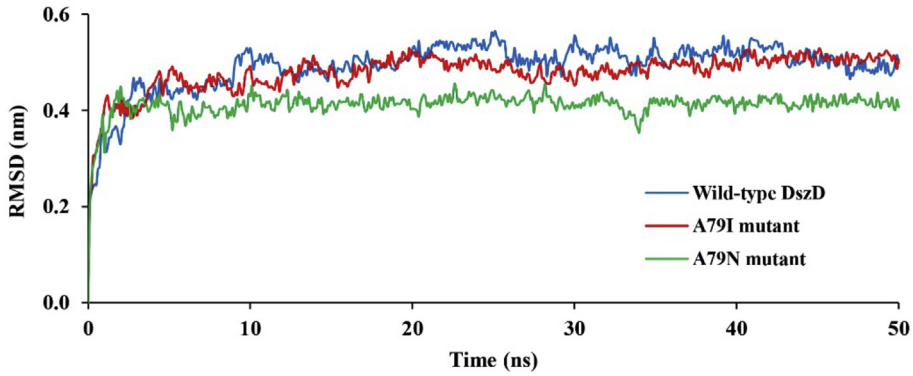

Fig. 3. RMSD of the C-α atoms as a function of time for the wild-type DszD enzyme, A79I mutant and A79N mutant in complex with FMN substrate.

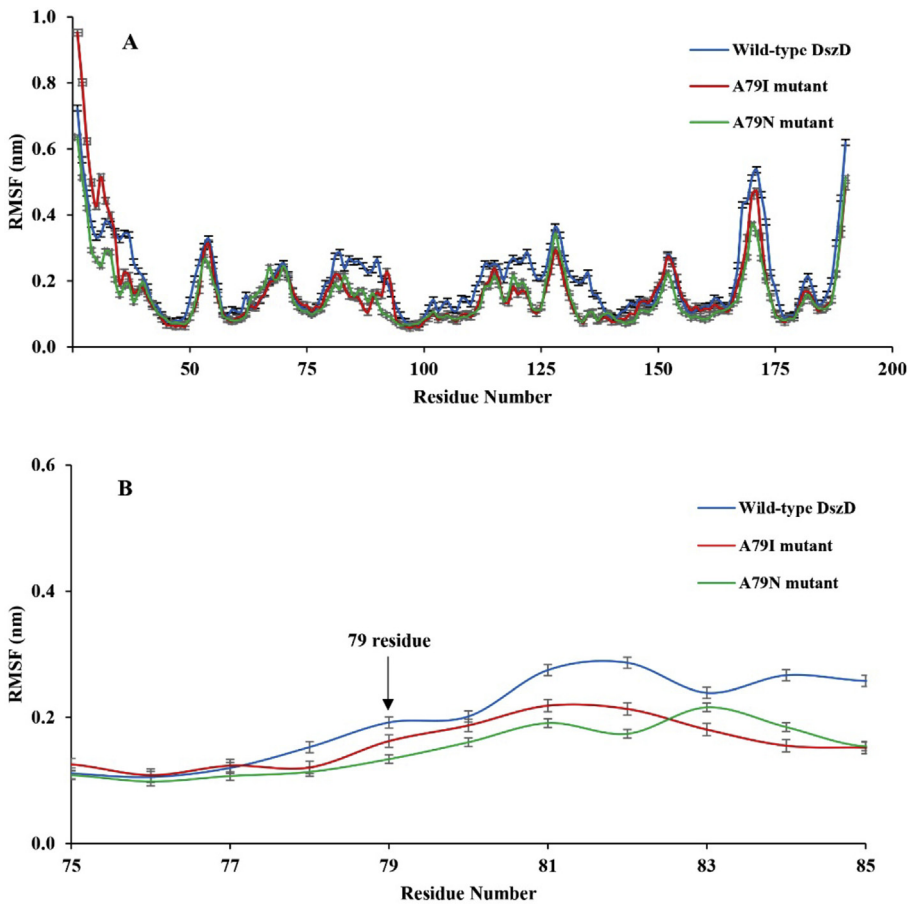

Fig. 4. Average RMSF of the C-α atoms as a function of residue for (A) whole residues and (B) 75–85 residues of the wild-type enzyme, A79I mutant and A79N mutant.

transferred to *E. coli* BL21 (DE3). Then, the transfected bacterial colonies were selected on LB agar plates supplemented with ampicillin.

The biochemical analysis of the expression step showed that all of the desired cloned enzymes were overexpressed and had a distinct band on a polyacrylamide gel with a calculated molecular mass of 22 kDa (Fig. 8A). Western blot analysis confirmed the presence of significant level expression of recombinant wild-type DszD enzyme, A79I, and A79N mutants (Fig. 8B) (see Fig. 7).

3.6. Oxidoreductase activity evaluation

In order to evaluate the mutated enzymes activity toward the biodesulfurization process in comparison with wild-type DszD enzyme, the oxidation rate of NADH was determined for both mutants and wild-type enzyme. The enzyme activity of the A79I and A79N mutants were respectively increased 1.9-fold and 2.3-fold compared to the recombinant wild-type enzyme (Table 6).

The increased activity of A79I could be attributed to the substitution of a methyl group in alanine 79 in wild-type enzyme with *Sec*-butyl group. The bigger alkyl group may help to the better insertion of substrate in the active site of the enzyme. Moreover, the alkyl groups are considered as electron donor groups which their electron donating feature increases by increasing the length of the alkyl group (Vollhardt and Schore, 2014). Hence, it could be concluded that may be by substitution of *Sec*-butyl instead of methyl group, the ability of NAD(P)H for reduction of FMN is increased by induction of more electron donoring

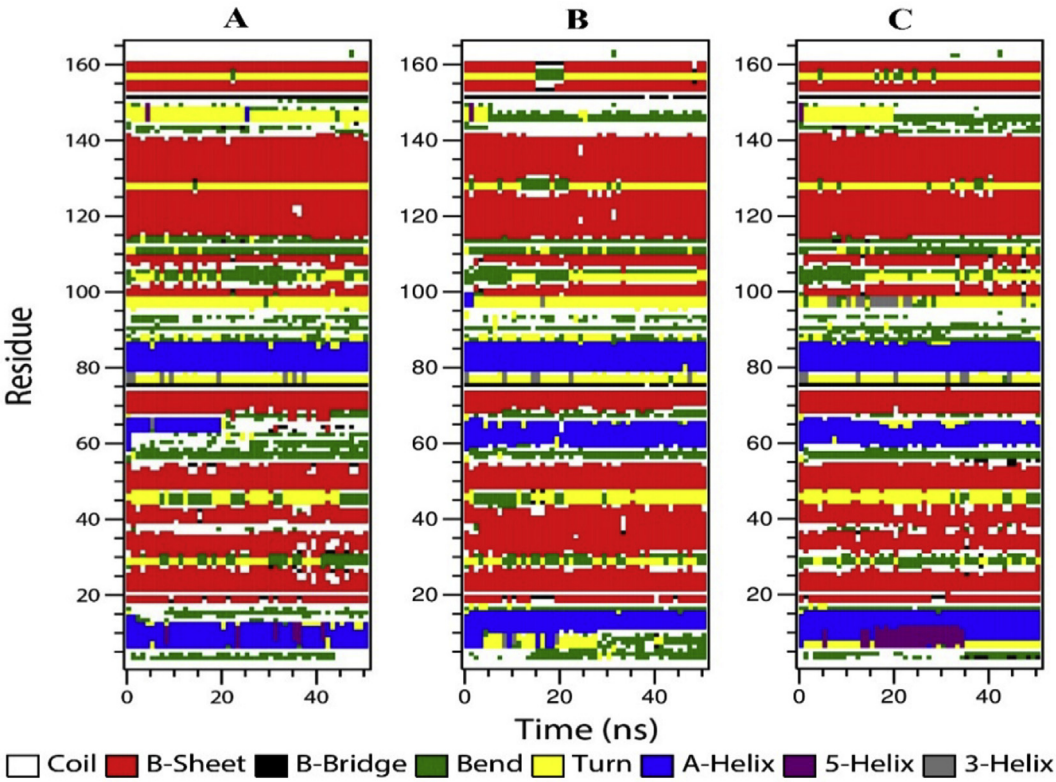

Fig. 5. DSSP analysis of (A) wild-type DszD enzyme (B) A79I and (C) A79N mutants.

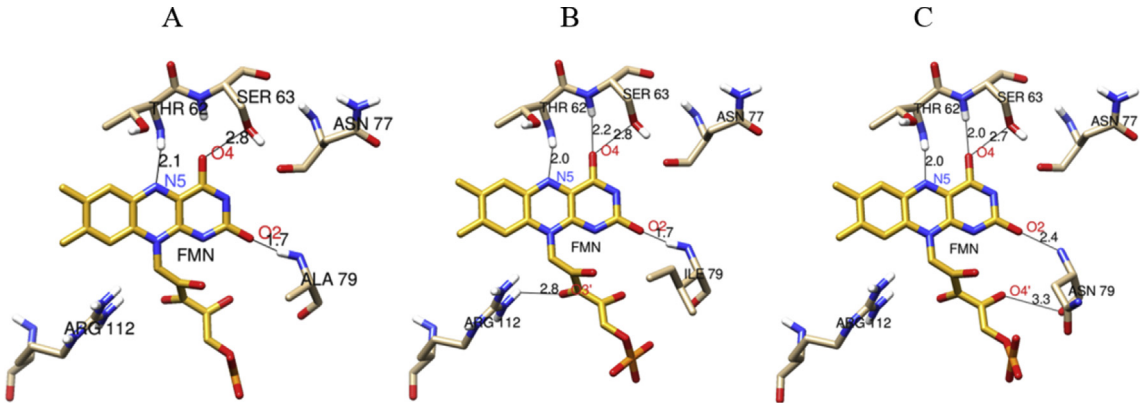

Fig. 6. Analysis of hydrogen bonds between FMN substrate and (A) wild-type DszD enzyme (B) A79I and (C) A79N using Chimera software.

Table 2
Hydrogen bond lengths between atoms of the wild-type DszD and mutants (A79I and A79N) with FMN substrate.

Residue	residue atom	FMN atom	The length of hydrogen bond (Å)		
			Wild-type DszD	A79I mutant	A79N mutant
Thr62	NH	N5	2.1	2.0	2.0
Ser63	NH	O4	-	2.2	2.0
Ser63	OG	O4	2.8	2.8	2.7
Ala79	NH	O2	1.7	-	-
Ile79	NH	O2	-	1.7	-
Asn79	NH	O2	-	-	2.4
Asn79	OH	O4′	-	-	3.3

from *Sec*-butyl side.

The increased catalytic activity of the A79N mutant is related to the presence of the more polar amide group in asparagine instead of the hydrogen atom in alanine, which causes to more effective electrostatic attraction between enzyme and FMN and also better insertion of polar FMN in the active site of the enzyme. These results are in accordance with calculated binding energies in Table 3, which shows that by substitution of alanine in wild-type enzyme by asparagine in A79N mutant, the van der Waals interaction has increased because of the dipole-dipole interaction (Table 3). These results demonstrate that DszD has a higher potential to increase the enzyme activity in the 4S pathway. So, the mutation on DszD enzyme and its participation in recombinant host cells such as *E. coli* or a recombinant *R. erythropolis* system can cause the better and more efficient biodesulfurization process.

Table 3
Average of binding free energy components obtained from MM-PBSA method for wild-type and mutants.

Interaction	Wild-type DszD (kcal/mol)	A79I (kcal/mol)	A79N (kcal/mol)
van der Waal energy	-26.41 ± 2.25	-24.57 ± 3.20	-35.24 ± 1.03
Electrostatic energy	10.07 ± 1.17	8.44 ± 1.89	10.58 ± 0.71
Polar solvation energy	11.46 ± 0.95	10.61 ± 2.82	12.12 ± 0.26
nonpolar solvation energy	-3.88 ± 0.63	-4.64 ± 1.12	-4.03 ± 0.25
Binding free energy	-8.76 ± 0.75	-10.16 ± 2.65	-16.57 ± 0.20

Table 4
Contribution of Ala79 residue in the total binding free energy for wild-type and mutants.

Wild-type DszD (kcal/mol)	A79I (kcal/mol)	A79N (kcal/mol)
-2.72 ± 0.73	-3.53 ± 0.17	-4.05 ± 0.35

Table 5
Wild-type and mutagenic primer sequences.

Primer	Primer sequence
DszD-F	ATGGATCCATGTCTGACAAGCCGAATGC
DszD-R	GTAGAATTCCTACTATTGACCTAACGGAGTCGG
A79I-R	GACGTCTC*AAT*GATGTTGAACG
A79I–F	CGTTCAACATC*ATT*GAGACGTC
A79N-R	GACGTCTCG*TTG*ATGTTGAACG
A79N–F	CGTTCAACATC*AAC*GAGACGTC

Table 6
Comparison of the activity between recombinant wild-type DszD enzyme and its mutants.

Enzyme	Specific activity (U/mg)	compared with the activity of the wild-type enzyme
Wild-type DszD enzyme	184	1
A79I mutant	352	1.9
A79N mutant	424	2.3

4. Conclusion

DszD enzyme participates in the 4S pathway, a process through which the organism *Rhodococcus erythropolis* strain IGTS8 is able to use DBT in crude oil and derivatives as a source of sulfur, without degrading the fuel value of the product. Despite promising, the larger-scale bio-desulfurization using IGTS8 has been limited by the rate at which bacterial cells can remove sulfur. In this study, we investigated the effect of manipulation in key residues on the enzymatic activity of the DszD by bioinformatics and experimental results. The applied methods revealed the key residues on the active site regions of the DszD enzyme molecule. Among the key residues, the alanine 79 has a critical role in the active site of the DszD enzyme. Furthermore, the bioinformatics and experimental results uniformly confirmed the higher specific activity of the A79I and A79N mutants compared to the wild-type DszD enzyme. Accordingly, the results can be used for an efficient bacterial desulfurization process.

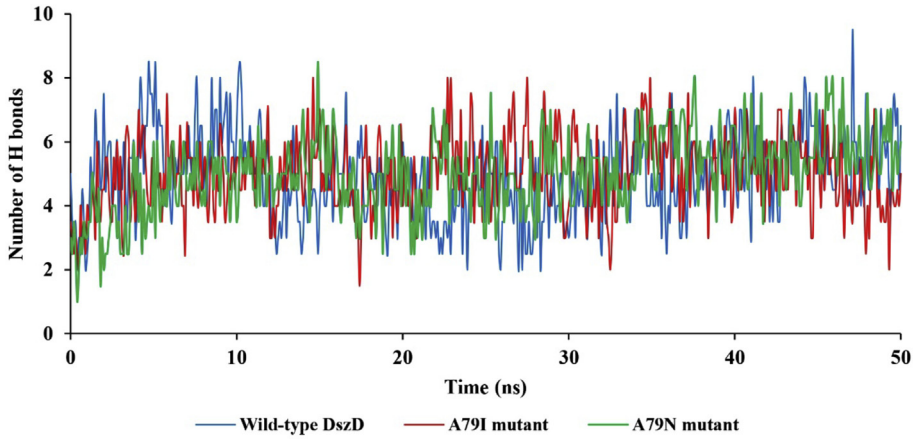

Fig. 7. The average number of H-bonds between FMN and enzymes during the 50 ns simulation.

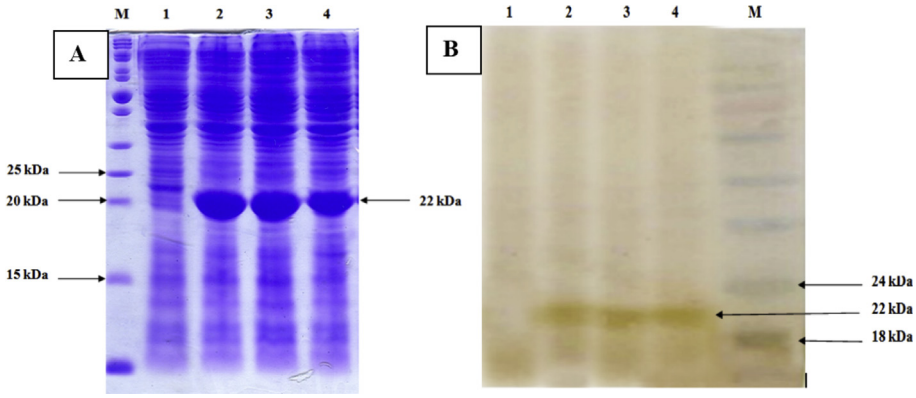

Fig. 8. (A) SDS–PAGE analysis of total cell proteins of non-transformed *E. coli* BL21, lane 1, and recombinant wild-type *R. erytropolis* IGTS8 DszD, A79N and A79I mutants, Lanes 2, 3 and 4, respectively (B) Western-blot analysis of the recombinants A79N and A79I. Lane 1 is negative control Lanes 2, 3 and 4 are recombinant wild-type DszD, A79N and A79I mutants, respectively. Lane M; Protein Molecular Weight Marker.

Declarations

Author contribution statement

Rramin Fallah: Performed the experiments; Analyzed and interpreted the data; Contributed reagents, materials, analysis tools or data; Wrote the paper.

Bijan Bambai: Conceived and designed the experiments; Analyzed and interpreted the data; Contributed reagents, materials, analysis tools or data; Wrote the paper.

Kasra Esfahani, Abbas Akhavan Sepahi: Analyzed and interpreted the data; Wrote the paper.

Funding statement

This research did not receive any specific grant from funding agencies in the public, commercial, or not-for-profit sectors.

Competing interest statement

The authors declare no conflict of interest.

Additional information

No additional information is available for this paper.

References

Abraham, M.J., Murtola, T., Schulz, R., Páll, S., Smith, J.C., Hess, B., Lindahl, E., 2015. GROMACS: high performance molecular simulations through multi-level parallelism from laptops to supercomputers. Software 1, 19–25.
Akhtar, N., Ghauri, M.A., Akhtar, K., 2016. Dibenzothiophene desulfurization capability and evolutionary divergence of newly isolated bacteria. Arch. Microbiol. 198, 509–519.
Berendsen, H.J., Postma, J.v., van Gunsteren, W.F., DiNola, A., Haak, J., 1984. Molecular dynamics with coupling to an external bath. J. Chem. Phys. 81, 3684–3690.
Borzenkova, N., Veselova, I., Shekhovtsova, T., 2013. Biochemical methods of crude hydrocarbon desulfurization. Biol. Bull. Rev. 3, 296–311.
Chen, S., Zhao, C., Liu, Q., Zang, M., Liu, C., Zhang, Y., 2018. Thermophilic biodesulfurization and its application in oil desulfurization. Appl. Microbiol. Biotechnol. 102, 9089–9103.
Darden, T., York, D., Pedersen, L., 1993. Particle mesh Ewald: an N· log (N) method for Ewald sums in large systems. J. Chem. Phys. 98, 10089–10092.
Davoodi-Dehaghani, F., Vosoughi, M., Ziaee, A.A., 2010. Biodesulfurization of dibenzothiophene by a newly isolated Rhodococcus erythropolis strain. Bioresour. Technol. 101, 1102–1105.
Etemadi, N., Sepahy, A.A., Mohebali, G., Yazdian, F., Omidi, M., 2018. Enhancement of bio-desulfurization capability of a newly isolated thermophilic bacterium using starch/iron nanoparticles in a controlled system. Int. J. Biol. Macromol. 120, 1801–1809.
Ferreira, P., Sousa, S.F., Fernandes, P.A., Ramos, M.J., 2017. Improving the catalytic power of the DszD enzyme for the biodesulfurization of crude oil and derivatives. Chem. A Eur. J. 23, 17231–17241.
Frishman, D., Argos, P., 1995. Knowledge-based protein secondary structure assignment. Proteins: Struct. Funct. Bioinf. 23, 566–579.
Genheden, S., Ryde, U., 2015. The MM/PBSA and MM/GBSA methods to estimate ligand-binding affinities. Expert Opin. Drug Discov. 10, 449–461.
Gupta, N., Roychoudhury, P., Deb, J., 2005. Biotechnology of desulfurization of diesel: prospects and challenges. Appl. Microbiol. Biotechnol. 66, 356–366.
Hess, B., 2008. P-LINCS: a parallel linear constraint solver for molecular simulation. J. Chem. Theory Comput. 4, 116–122.
Kabsch, W., Sander, C., 1983. Dictionary of protein secondary structure: pattern recognition of hydrogen-bonded and geometrical features. Biopolym. Orig. Res. Biomole. 22, 2577–2637.
Kamali, N., Tavallaie, M., Bambai, B., Karkhane, A.A., Miri, M., 2010. Site-directed mutagenesis enhances the activity of NADH-FMN oxidoreductase (DszD) activity of Rhodococcus erythropolis. Biotechnol. Lett. 32, 921–927.
Kaplan, W., Littlejohn, T.G., 2001. Swiss-PDB viewer (deep view). Briefings Bioinf. 2, 195–197.
Karimi, E., Yazdian, F., Rasekh, B., Jeffryes, C., Rashedi, H., Sepahi, A.A., Shahmoradi, S., Omidi, M., Azizi, M., Bidhendi, M.E., 2018. DBT desulfurization by decorating bacteria using modified carbon nanotube. Fuel 216, 787–795.
Khosravinia, S., Mahdavi, M.A., Gheshlaghi, R., Dehghani, H., Rasekh, B., 2018. Construction and characterization of a new recombinant vector to remove sulfate repression of dsz promoter transcription in biodesulfurization of dibenzothiophene. Front. Microbiol. 9.
Kilbane II, J.J., 2006. Microbial biocatalyst developments to upgrade fossil fuels. Curr. Opin. Biotechnol. 17, 305–314.
Koziara, K.B., Stroet, M., Malde, A.K., Mark, A.E., 2014. Testing and validation of the Automated Topology Builder (ATB) version 2.0: prediction of hydration free enthalpies. J. Comput. Aided Mol. Des. 28, 221–233.
Kruger, N.J., 2002. The Bradford Method for Protein Quantitation. The Protein Protocols Handbook. Springer, pp. 15–21.
Kumari, R., Kumar, R., Consortium, O.S.D.D., Lynn, A., 2014. g_mmpbsa-A GROMACS tool for high-throughput MM-PBSA calculations. J. Chem. Inf. Model. 54, 1951–1962.
Mark, P., Nilsson, L., 2001. Structure and dynamics of the TIP3P, SPC, and SPC/E water models at 298 K. J. Phys. Chem. A 105, 9954–9960.
Martínez, I., Mohamed, M.E.-S., Santos, V.E., García, J.L., García-Ochoa, F., Díaz, E., 2017. Metabolic and process engineering for biodesulfurization in Gram-negative bacteria. J. Biotechnol. 262, 47–55.
Morris, G.M., Huey, R., Lindstrom, W., Sanner, M.F., Belew, R.K., Goodsell, D.S., Olson, A.J., 2009. AutoDock4 and AutoDockTools4: automated docking with selective receptor flexibility. J. Comput. Chem. 30, 2785–2791.
Morrison, E., Kantz, A., Gassner, G.T., Sazinsky, M.H., 2013. Structure and mechanism of styrene monooxygenase reductase: new insight into the FAD-transfer reaction. Biochemistry 52, 6063–6075.
Nazari, F., Kefayati, M., Raheb, J., 2017. The study of biological technologies for the removal of sulfur compounds. J. Sci. Islam. Repub. Iran 28, 205–219.
Nielsen, M., Lundegaard, C., Lund, O., Petersen, T.N., 2010. CPHmodels-3.0—remote homology modeling using structure-guided sequence profiles. Nucleic Acids Res. 38, W576–W581.
Nuhu, A.A., 2013. Bio-catalytic desulfurization of fossil fuels: a mini review. Rev. Environ. Sci. Biotechnol. 12, 9–23.
Oostenbrink, C., Villa, A., Mark, A.E., Van Gunsteren, W.F., 2004. A biomolecular force field based on the free enthalpy of hydration and solvation: the GROMOS force-field parameter sets 53A5 and 53A6. J. Comput. Chem. 25, 1656–1676.
Parrinello, M., Rahman, A., 1981. Polymorphic transitions in single crystals: a new molecular dynamics method. J. Appl. Phys. 52, 7182–7190.
Sambrook, J., Fritsch, E.F., Maniatis, T., 1989. Molecular Cloning: a Laboratory Manual. Cold spring harbor laboratory press.
Schägger, H., 2006. Tricine–sds-page. Nat. Protoc. 1, 16.
Sousa, S.r.F., Sousa, J.F., Barbosa, A.C., Ferreira, C.E., Neves, R.P., Ribeiro, A.n.J., Fernandes, P.A., Ramos, M.J.o., 2016. Improving the biodesulfurization of crude oil and derivatives: a QM/MM investigation of the catalytic mechanism of NADH-FMN oxidoreductase (DszD). J. Phys. Chem. A 120, 5300–5306.
Sucharitakul, J., Tinikul, R., Chaiyen, P., 2014. Mechanisms of reduced flavin transfer in the two-component flavin-dependent monooxygenases. Arch. Biochem. Biophys. 555, 33–46.
Tripathi, S., Srivastava, G., Sharma, A., 2016. Molecular dynamics simulation and free energy landscape methods in probing L215H, L217R and L225M βI-tubulin mutations causing paclitaxel resistance in cancer cells. Biochem. Biophys. Res. Commun. 476, 273–279.
Vollhardt, K.P.C., Schore, N.E., 2014. Organic Chemistry; Palgrave Version: Structure and Function. Macmillan International Higher Education.
Xiao, J., Wang, X., Fujii, M., Yang, Q., Song, C., 2013. A novel approach for ultra-deep adsorptive desulfurization of diesel fuel over TiO2–CeO2/MCM-48 under ambient conditions. AIChE J. 59, 1441–1445.
Young, L., Smith, H.O., Gibson, D.G., 2017. Vitro Recombination Method. Google Patents.
Zhang, M., Zhu, W., Xun, S., Li, H., Gu, Q., Zhao, Z., Wang, Q., 2013. Deep oxidative desulfurization of dibenzothiophene with POM-based hybrid materials in ionic liquids. Chem. Eng. J. 220, 328–336.